Impaired Autophagy in the Lipid-Storage Disorder Niemann-Pick Type C1 Disease

Sovan Sarkar,[1] Bernadette Carroll,[2] Yosef Buganim,[1] Dorothea Maetzel,[1] Alex H.M. Ng,[3] John P. Cassady,[1] Malkiel A. Cohen,[1] Souvik Chakraborty,[4] Haoyi Wang,[1] Eric Spooner,[1] Hidde Ploegh,[1] Joerg Gsponer,[3] Viktor I. Korolchuk,[2] and Rudolf Jaenisch[1,*]

[1]Whitehead Institute for Biomedical Research, Massachusetts Institute of Technology, 9 Cambridge Center, Cambridge, MA 02142, USA
[2]Institute for Ageing and Health, Newcastle University, Campus for Ageing and Vitality, Newcastle upon Tyne NE4 5PL, UK
[3]Department of Biochemistry and Molecular Biology, Centre for High-Throughput Biology, University of British Columbia, Vancouver, BC V6T 1Z4, Canada
[4]Department of Pediatrics, University of Pittsburgh School of Medicine, Children's Hospital of Pittsburgh of UPMC, Pittsburgh, PA 15224, USA
*Correspondence: jaenisch@wi.mit.edu
http://dx.doi.org/10.1016/j.celrep.2013.10.042

SUMMARY

Autophagy dysfunction has been implicated in misfolded protein accumulation and cellular toxicity in several diseases. Whether alterations in autophagy also contribute to the pathology of lipid-storage disorders is not clear. Here, we show defective autophagy in Niemann-Pick type C1 (NPC1) disease associated with cholesterol accumulation, where the maturation of autophagosomes is impaired because of defective amphisome formation caused by failure in SNARE machinery, whereas the lysosomal proteolytic function remains unaffected. Expression of functional NPC1 protein rescues this defect. Inhibition of autophagy also causes cholesterol accumulation. Compromised autophagy was seen in disease-affected organs of *Npc1* mutant mice. Of potential therapeutic relevance is that HP-β-cyclodextrin, which is used for cholesterol-depletion treatment, impedes autophagy, whereas stimulating autophagy restores its function independent of amphisome formation. Our data suggest that a low dose of HP-β-cyclodextrin that does not perturb autophagy, coupled with an autophagy inducer, may provide a rational treatment strategy for NPC1 disease.

INTRODUCTION

Autophagy, an intracellular degradation pathway for aggregation-prone proteins and damaged organelles, is essential for cellular homeostasis. This dynamic process, defined as autophagic flux, encompasses the generation of autophagosomes and its fusion with late endosomes to form amphisomes, which subsequently fuse with lysosomes forming autolysosomes for degrading its cargo (Figure S1A). Starvation induces autophagy for maintaining energy homeostasis by recycling of cytosolic components (Ravikumar et al., 2010). Tissue-specific abrogation of constitutive autophagy, such as by deletion of essential autophagy genes *Atg5* or *Atg7*, in the brain or liver of mice in the absence of any pathogenic protein results in degeneration in the affected organs, suggesting that impaired autophagy contributes to the disease-related phenotypes in neurodegenerative and liver diseases (Hara et al., 2006; Komatsu et al., 2006, 2007). Thus, compromised autophagy is attributable to the etiology of several neurodegenerative disorders and certain liver diseases where upregulation of autophagy is considered beneficial (Meijer and Codogno, 2006; Mizushima et al., 2008; Rubinsztein et al., 2012; Sarkar, 2013).

Autophagy also regulates the metabolism of lipids including cholesterol (Singh et al., 2009), which are essential structural components of membranes and govern intracellular trafficking (Ikonen, 2008). Niemann-Pick type C1 (NPC1) disease, associated with neurodegeneration and liver dysfunction, is characterized by cholesterol accumulation in the late endosomal/lysosomal (LE/L) compartments resulting from disease-causing mutations primarily in the NPC1 protein (Karten et al., 2009; Rosenbaum and Maxfield, 2011). The transmembrane NPC1 protein comprises five sterol-sensing domains, possibly mediating cholesterol efflux from late endosomes (Higgins et al., 1999; Kwon et al., 2009). How alterations in cholesterol homeostasis in lipid-storage disorders might perturb autophagy is not completely understood. Here, we show defective autophagic flux in NPC1 disease, in which stimulation of autophagy restores the function of the pathway.

RESULTS

Accumulation of Autophagosomes in NPC1 Mutant Cells Is due to a Block in Autophagic Flux

We initially confirmed accumulation of cholesterol and lipids by Filipin and BODIPY staining in NPC1 patient fibroblasts, in
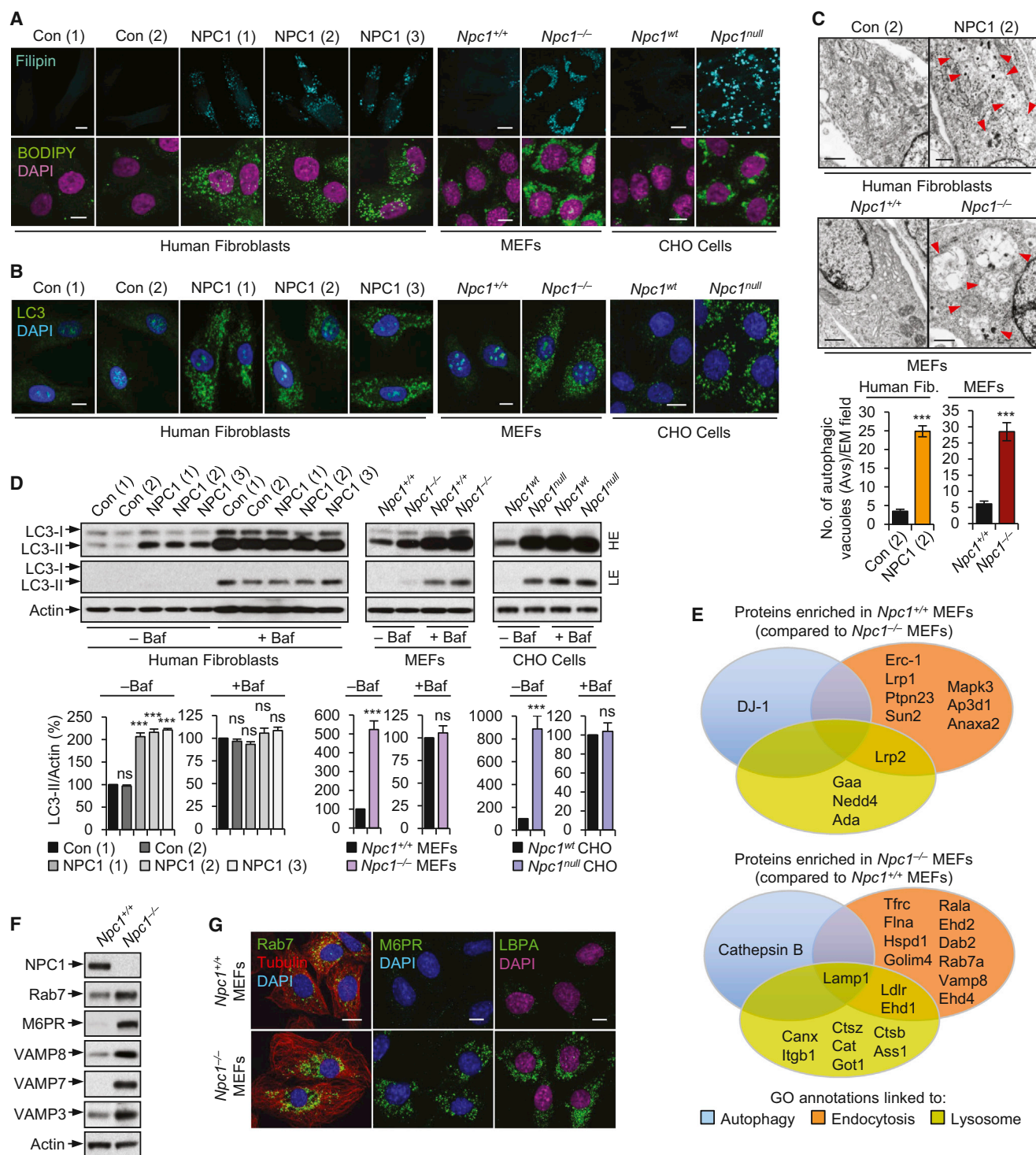
Figure 1. Accumulation of Autophagosomes in NPC1 Mutant Cells Is due to a Block in Autophagic Flux

(A and B) Filipin and BODIPY fluorescence staining (A) and immunofluorescence staining with anti-LC3 antibody (B) in control (Con) and NPC1 patient fibroblasts, $Npc1^{+/+}$ and $Npc1^{-/-}$ MEFs, and in $Npc1^{wt}$ and $Npc1^{null}$ CHO-K1 cells are shown. Details of control and NPC1 patient fibroblast lines are listed in Figure S1B. The scale bars represent 10 μm. See also Figure S1D.

(C) Electron microscopy (EM) images and quantification of autophagic vacuoles in control and NPC1 patient fibroblasts (fib), and in $Npc1^{+/+}$ and $Npc1^{-/-}$ MEFs, are shown. The scale bars represent 500 nm. See also Figures S1E and S1F.

(D) Immunoblot analyses with anti-LC3 and anti-actin antibodies in control and NPC1 patient fibroblasts, $Npc1^{+/+}$ and $Npc1^{-/-}$ MEFs, and in $Npc1^{wt}$ and $Npc1^{null}$ CHO-K1 cells treated with or without 400 nM bafA$_1$ (Baf) for 4 hr are shown. High exposure (HE) and low exposure (LE) of the same immunoblot are shown.

(legend continued on next page)

$Npc1^{-/-}$ MEFs from $npc1^{nih}$ mutant mice exhibiting NPC1 clinical abnormalities (Loftus et al., 1997), and in Chinese hamster ovary-K1 (CHO-K1) cells containing a deletion in the $Npc1$ locus ($Npc1^{null}$) (Millard et al., 2000) (Figures 1A and S1B). In these NPC1 mutant cells, the NPC1 protein was either low or not detected (Figure S1C). Perturbation in autophagy was measured by the steady-state number of autophagosomes, which correlates with the autophagosome-associated form of microtubule-associated protein 1 light-chain 3 (LC3-II) (Kabeya et al., 2000; Klionsky et al., 2012). We found accumulation of autophagosomes in the NPC1 mutant cells, as assessed by elevated LC3-II levels and LC3+ vesicles, including autophagic vacuoles analyzed by electron microscopy (Figures 1B, 1C, and S1C– S1F). Previous studies have attributed this increase in the steady-state number of autophagosomes in NPC1 disease to activation of autophagy (Ishibashi et al., 2009; Ordonez et al., 2012; Pacheco et al., 2007). Because both synthesis and degradation affect steady-state LC3-II levels, we determined autophagic flux using bafilomycin A₁ (bafA₁), which prevents lysosomal acidification and accumulates LC3-II by inhibiting its degradation. In bafA₁-treated conditions, an autophagy inducer increases LC3-II levels, whereas an autophagy blocker has no change compared to controls (Klionsky et al., 2012; Sarkar et al., 2009) (see Supplemental Experimental Procedures). Despite significant LC3-II accumulation in NPC1 mutant cells compared to controls, this difference was no longer detected following bafA₁ treatment (Figure 1D). Thus, in contrast to previous studies by Ishibashi et al. (2009), Ordonez et al. (2012), and Pacheco et al. (2007), our data suggest that LC3-II accumulation is not due to increased autophagosome synthesis but rather is caused by impaired degradation of autophagosomes.

Defective Amphisome Formation in NPC1 Mutant Cells due to Impaired Recruitment of Components of the SNARE Machinery to Late Endosomes

To gain mechanistic insights, we performed mass spectrometry (MS) analyses in $Npc1$ MEFs. Gene Ontology (GO) annotations indicated changes in intracellular transport in $Npc1^{-/-}$ MEFs when compared to $Npc1^{+/+}$ MEFs (Figures S1G and S1H). We analyzed genes with a significant difference in expression levels and GO annotations linked to autophagy, endocytosis, or lysosomes (Figure 1E). For example, Rab7, a late endosome-resident GTPase regulating endosomal/autophagosomal maturation (Jäger et al., 2004; Stenmark, 2009), was enriched in $Npc1^{-/-}$ MEFs. We confirmed an elevation of Rab7, and other late endosome markers, such as cation-independent mannose-6-phosphate receptor (M6PR) and lysobisphosphatidic acid (LBPA) (Kobayashi et al., 1999), suggesting accumulation of late endosomes in NPC1 mutant cells (Figures 1E–1G, S1I, and S1J).

Because the loss of NPC1 protein from LE/L compartments in NPC1 mutant cells (Carstea et al., 1997; Higgins et al., 1999; Karten et al., 2009) leads to increase in autophagosomes (LC3+) and late endosomes (Rab7+), we investigated the formation of amphisomes arising due to fusion of these vesicular compartments (Berg et al., 1998). Although starvation increases their number in control cells (Jäger et al., 2004), EGFP-LC3+/mRFP-Rab7+ amphisomes were significantly reduced in $Npc1^{-/-}$ MEFs both under basal (full medium [FM]) and starvation (HBSS) conditions (Figures 2A and S2A), suggesting impaired formation of amphisome in NPC1 mutant cells. Further analyzing this process with endogenous LC3+ and Rab7+ vesicles revealed a similar defect in starved $Npc1^{-/-}$ MEFs (Figure S2B). Additionally, using FITC-conjugated dextran that undergoes cellular uptake through the endocytic pathway, NPC1 mutant cells exhibited significantly less amphisomes as assessed by FITC-dextran+/mRFP-LC3+ colocalization (Figures 2B and S2C).

The defect in autophagosome-late endosome fusion could be due to perturbations in the formation of specific SNARE complexes, such as between autophagosomal syntaxin 17 (Stx17) and LE/L VAMP8 mediated by SNAP-29 (Itakura et al., 2012). Despite an increase in VAMP8 levels in $Npc1^{-/-}$ MEFs, as revealed by MS data (Figures 1E, 1F, and S1I), the fusion between Myc-Stx17+ autophagosomes and FLAG-VAMP8+ vesicles, as well as coimmunoprecipitation between these SNARE proteins, was significantly decreased both under basal and starvation conditions as compared to $Npc1^{+/+}$ MEFs (Figures 2C and 2D). We found impaired localization of VAMP8 to mRFP-Rab7+ late endosomes in $Npc1^{-/-}$ MEFs, possibly contributing to this defect in forming SNARE complex (Figures 2E and S2D). Other SNARE proteins implicated in autophagosome maturation include VAMP3 (regulates amphisome formation) and VAMP7 (regulates fusion with lysosomes) (Fader et al., 2009), which were elevated in $Npc1^{-/-}$ MEFs (Figures 1F and S1I). Similar to VAMP8, localization of EGFP-VAMP3, but not of EGFP-VAMP7, to mRFP-Rab7+ late endosomes was reduced in $Npc1^{-/-}$ MEFs (Figures 2F and S2E). Consistently, the localization of autophagosomal Myc-Stx17+ to late endocytic Rab7+ vesicles, which is an indication of amphisome formation during starvation as seen in $Npc1^{+/+}$ MEFs, was significantly reduced in $Npc1^{-/-}$ MEFs (Figures 2G and S2F). Thus, the inability to recruit multiple components of the SNARE machinery to late endosomes in NPC1 mutant cells impairs amphisome formation.

Impaired Autophagosome Maturation in NPC1 Mutant Cells Retards Autophagic Cargo Clearance

Defective amphisome formation will affect the maturation of autophagosomes into autolysosomes. We analyzed this process using tandem fluorescent-tagged mRFP-GFP-LC3 reporter where autophagosomes emit both mRFP/GFP signals, but

---

(E) GO enrichments among differentially expressed genes with enriched abundance in $Npc1^{+/+}$ and $Npc1^{-/-}$ MEFs that have GO annotations linking them to autophagy (blue), the lysosomal (green), and the endosomal system (orange) are shown. See also Figures S1G and S1H.

(F) Immunoblot analyses with anti-NPC1, anti-Rab7, anti-M6PR, anti-VAMP8, anti-VAMP7, anti-VAMP3, and anti-actin antibodies in $Npc1^{+/+}$ and $Npc1^{-/-}$ MEFs are shown. See also Figure S1I.

(G) Immunofluorescence staining with anti-Rab7, anti-tubulin, anti-M6PR, and anti-LBPA antibodies in $Npc1^{+/+}$ and $Npc1^{-/-}$ MEFs is shown. The scale bars represent 10 μm.

Graphical data denote mean ± SEM. ***$p < 0.001$. ns, nonsignificant.
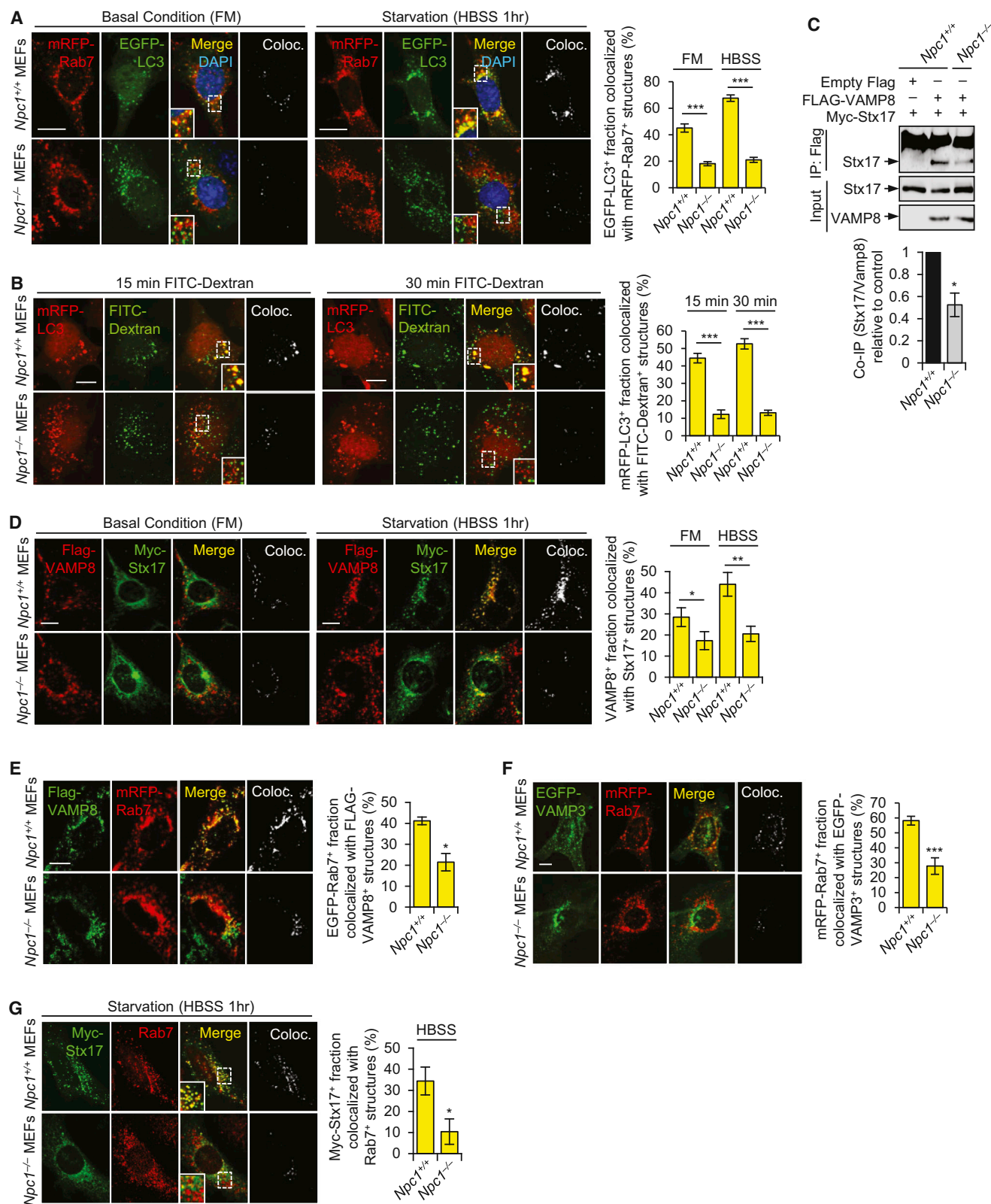
(legend on next page)

autolysosomes emit only an acid-stable mRFP signal because the pH-sensitive GFP signal is quenched in acidic lysosomes (Kimura et al., 2007). Unlike control cells displaying autolysosomes (mRFP$^+$-GFP$^-$-LC3), the majority of accumulated vesicles in NPC1 mutant cells were autophagosomes (mRFP$^+$-GFP$^+$-LC3) (Figures 3A and S3A), suggesting a defect in autophagosome maturation. Consequently, the clearance of p62, a specific autophagy substrate (Pankiv et al., 2007), was decreased in NPC1 mutant cells, leading to its accumulation and aggregation that costained with LC3$^+$ vesicles (Figures 3B, 3C, S3B, and S3C). Using tandem fluorescent-tagged mCherry-GFP-p62 reporter (Pankiv et al., 2007), we found that the majority of p62 aggregates in $Npc1^{-/-}$ MEFs were autophagosome associated (mCherry$^+$-GFP$^+$-p62), in contrast to those in controls that were mostly autolysosome associated (mCherry$^+$-GFP$^-$-p62 aggregates) (Figure 3D).

Although the levels of p62 in $Npc1^{-/-}$ MEFs were comparable to that in autophagy-deficient $Atg5^{-/-}$ MEFs (Figure S3D) that do not have autophagosomes/LC3-II (Kuma et al., 2004), bafA$_1$ treatment further increased p62 levels in $Npc1^{-/-}$ MEFs (Figure S3E). Moreover, the kinetics of endogenous p62 degradation in the presence of cycloheximide (inhibitor of protein translation) was substantially slower in $Npc1^{-/-}$ MEFs compared to $Npc1^{+/+}$ MEFs, whereas no clearance of p62 occurred in $Atg5^{-/-}$ MEFs (Figures 3E and S3F). These data suggest that the impairment in autophagic flux in NPC1 mutant cells is not absolute.

Consistent with effects that are associated with autophagy impairment, aggregation of mutant huntingtin (EGFP-HDQ74), an autophagy substrate (Ravikumar et al., 2004), and ubiquitylated proteins (Korolchuk et al., 2009) were increased in NPC1 mutant cells (Figures S3G and S3H). Autophagy also removes damaged mitochondria (mitophagy) (Youle and Narendra, 2011). Defective autophagy in $Npc1^{-/-}$ MEFs increased mitochondrial load, as assessed by elevated levels of Tom20, a translocase of outer mitochondrial membrane (Figure 3F). Furthermore, the MS data revealing decreased DJ-1 levels were confirmed in NPC1 mutant cells (Figures 1E, 3F, and S3I), an effect associated with mitochondrial fragmentation and accumulation of autophagosomes (Thomas et al., 2011). Indeed, NPC1 knockdown causes mitochondrial fragmentation (Ordo-

nez et al., 2012), which we verified in $Npc1^{-/-}$ MEFs (Figure S3J). Our data link NPC1 deficiency to defective mitophagy, a phenomenon linked to increased susceptibility to proapoptotic insults (Ravikumar et al., 2006; Youle and Narendra, 2011). Consequently, treatment with carbonyl cyanide m-chlorophenyl-hydrazone (CCCP), an uncoupler of mitochondrial membrane potential, substantially increased cell death in $Npc1^{-/-}$ MEFs compared to $Npc1^{+/+}$ MEFs (Figure 3G).

Upstream events regulating autophagosome biogenesis (Ravikumar et al., 2010), such as Atg5-Atg12 conjugation and phagophore formation (Atg16$^+$ vesicles), including beclin 1 and mTOR activity remained constant (Figures S1A and S3K–S3M). Thus, contrary to previous reports suggesting autophagy activation in NPC1 disease (Ishibashi et al., 2009; Ordonez et al., 2012; Pacheco et al., 2007), our data are consistent with autophagosome accumulation being due to a block in autophagic flux late in the pathway.

NPC1 Mutant Cells Exhibit No Overt Defects in Endocytic Cargo Degradation and Lysosomal Proteolytic Function

Because NPC1 mutant cells exhibit accumulation of late endosomes, we examined any perturbations in endocytic traffic by the uptake of FITC-dextran and its colocalization with LysoTracker$^+$ LE/L compartments. Although FITC-dextran and LysoTracker$^+$ vesicles accumulated in $Npc1^{-/-}$ MEFs, the fraction localizing with LysoTracker$^+$ vesicles was comparable with the control cells (Figure 3H). We also assessed clathrin-mediated endocytic degradation of epidermal growth factor receptor (EGFR). Despite elevated EGFR levels in NPC1 mutant cells, the rate of EGF-induced EGFR degradation was comparable to that of control cells (Figure S3N), suggesting that endocytic trafficking and lysosomal proteolysis are not compromised. Consistent with data in $Npc1^{-/-}$ mouse brain (Sleat et al., 2012), we confirmed increased LAMP1, and mature cathepsin B and cathepsin D levels as revealed by MS data, suggesting an accumulation of lysosomes and lysosomal proteases (Figures 1E, 3I, and 3J). Furthermore, cathepsin B activity was increased in $Npc1^{-/-}$ MEFs, although no significant alterations were found in NPC1 patient fibroblasts, compared to the respective control cells (Figure 3K). In contrast to an earlier

Figure 2. Perturbation of SNARE Machinery on Late Endosomes Impairs Amphisome Formation in NPC1 Mutant Cells

(A) Fluorescence staining and quantification of colocalization (Coloc.) of mRFP-Rab7$^+$ and EGFP-LC3$^+$ vesicles (an indication of amphisome formation) in $Npc1^{+/+}$ and $Npc1^{-/-}$ MEFs, expressing *mRFP-Rab7* and *EGFP-LC3* for 24 hr and cultured under basal (FM) and starvation (HBSS; last 1 hr) conditions, are shown. The scale bars represent 10 μm. See also Figure S2A.

(B) Fluorescence staining and quantification of colocalization of mRFP-LC3$^+$ and FITC-dextran$^+$ structures in $Npc1^{+/+}$ and $Npc1^{-/-}$ MEFs, expressing *mRFP-LC3* for 24 hr and then incubated in HBSS with Alexa Fluor 488 (FITC)-conjugated dextran for 15 or 30 min, are shown. The scale bars represent 10 μm. See also Figure S2C.

(C) Coimmunoprecipitation (coIP) of FLAG-Vamp8 and Myc-Syntaxin17 (Stx17) in $Npc1^{+/+}$ and $Npc1^{-/-}$ MEFs, expressing *Myc-Syntaxin17* and either empty vector or *FLAG-VAMP8* for 24 hr, then lysed and immunoprecipitated (IP) with anti-FLAG beads, is shown. Immunoblotting analysis with anti-Myc and anti-FLAG was done on inputs (with equal loading) and immunoprecipitated fractions.

(D) Fluorescence staining and quantification of colocalization of FLAG-VAMP8$^+$ and Myc-Syntaxin17$^+$ (Stx17) structures in $Npc1^{+/+}$ and $Npc1^{-/-}$ MEFs, expressing *FLAG-VAMP8* and *Myc-Syntaxin17* for 24 hr under basal (FM) and starvation (HBSS; last 1 hr) conditions, are shown. The scale bars represent 10 μm.

(E and F) Fluorescence staining and quantification of colocalization of FLAG-VAMP8$^+$ (E) or EGFP-VAMP3$^+$ (F) structures with mRFP-Rab7$^+$ vesicles in $Npc1^{+/+}$ and $Npc1^{-/-}$ MEFs, expressing *mRFP-Rab7* and either *FLAG-VAMP8* (E) or *EGFP-VAMP3* (F) for 24 hr in FM, are shown. The scale bars represent 10 μm.

(G) Immunofluorescence staining with anti-Rab7 antibody and quantification of colocalization of Rab7$^+$ and Myc-Syntaxin17$^+$ (Stx17) structures in $Npc1^{+/+}$ and $Npc1^{-/-}$ MEFs, expressing *Myc-Syntaxin17* for 24 hr in FM and then starved in HBSS for the last 1 hr, are shown. The scale bars represent 10 μm.

Graphical data denote mean ± SEM. ***p < 0.001, **p < 0.01, and *p < 0.05.
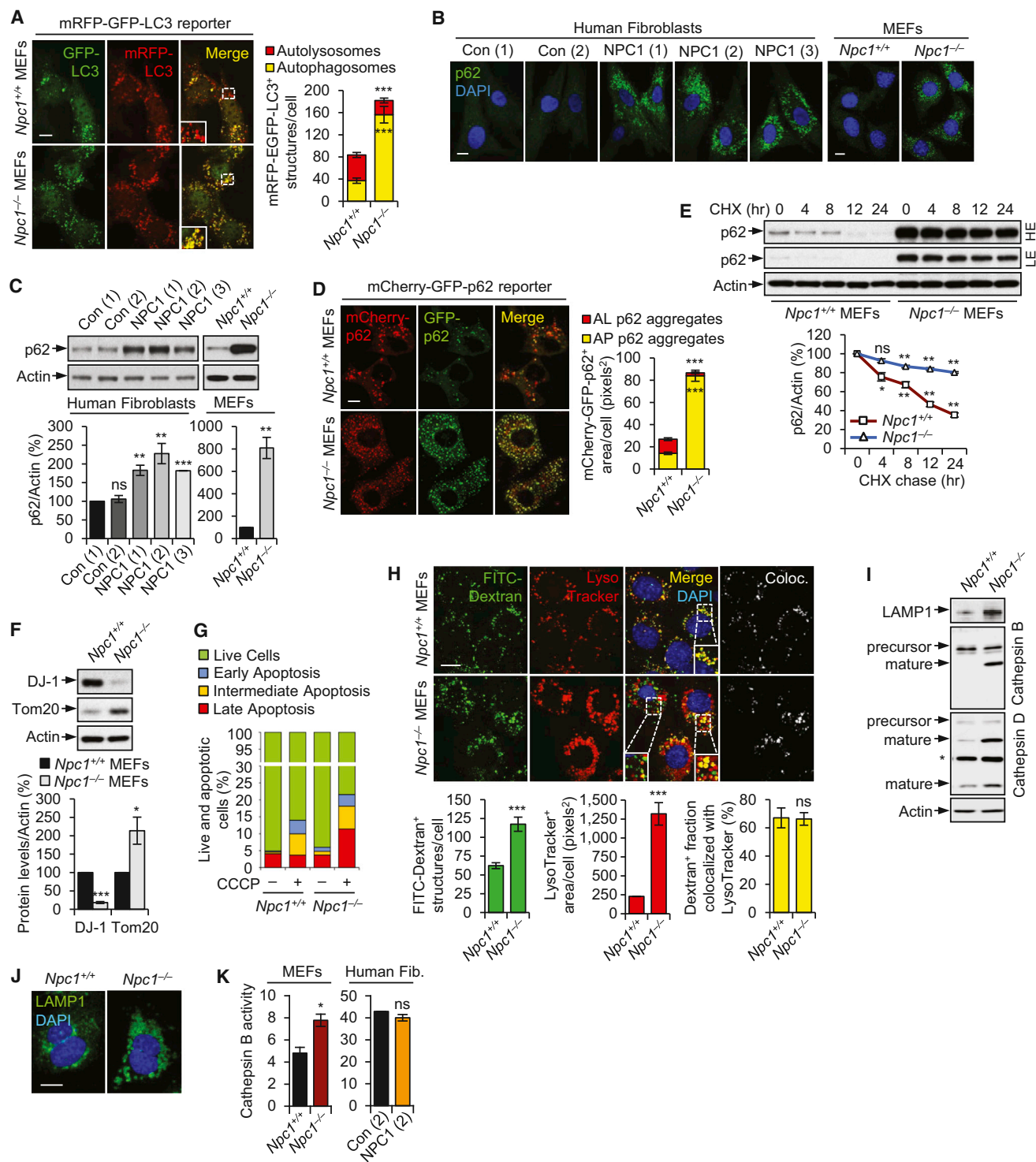
Figure 3. Impaired Autophagosome Maturation Retards Autophagic Cargo Clearance in NPC1 Mutant Cells that Are Associated with Defective Mitophagy, whereas Lysosomal Proteolysis Is Not Perturbed

(A) Fluorescence staining and quantification of autophagosomes (mRFP$^+$-GFP$^+$-LC3) and autolysosomes (mRFP$^+$-GFP$^-$-LC3) in $Npc1^{+/+}$ and $Npc1^{-/-}$ MEFs, expressing *mRFP-GFP-LC3* reporter for 24 hr, are shown. The scale bar represents 10 μm.

(B) Immunofluorescence staining with anti-p62 antibody in control and NPC1 patient fibroblasts, and in $Npc1^{+/+}$ and $Npc1^{-/-}$ MEFs, are shown. Quantification of the percentage of NPC1 mutant cells exhibiting increased p62$^+$ aggregates is shown in the scale bar represents Figure S3B. The scale bar represents 10 μm.

(C) Immunoblot analysis with anti-p62 and anti-actin antibodies in control and NPC1 patient fibroblasts, and in $Npc1^{+/+}$ and $Npc1^{-/-}$ MEFs, is shown.

(legend continued on next page)

report attributing impaired cathepsin activation to autophagy deregulation (Elrick et al., 2012), our data imply no obvious impairment in the lysosomal proteolytic function.

Functional NPC1 Protein Rescues the Autophagy Defects in NPC1 Mutant Cells, whereas Cholesterol-Depletion Treatment with HP-β-Cyclodextrin Blocks Autophagic Flux

Expression of functional NPC1 protein corrected the cholesterol phenotype in NPC1 mutant cells (Carstea et al., 1997). We found that overexpression of NPC1-EGFP in $Npc1^{-/-}$ MEFs also rescued the autophagy defects, as assessed by a reduction in p62 and LC3-II levels, and clearance of p62$^+$ aggregates, LC3$^+$ and LysoTracker$^+$ vesicles when compared to EGFP-transfected mutant cells (Figures 4A–4C and S4A). Consistent with NPC1 protein mediating vesicular traffic, transient expression of NPC1-EGFP that partially colocalized with mRFP-LC3$^+$ vesicles subtly increased autophagosome synthesis, as measured by increased LC3-II levels with or without bafA$_1$ (Figures S4B and S4C). This is likely due to a compensatory signal sensing NPC1 protein-mediated increased autophagic flux causing rapid clearance of autophagosomes.

Cholesterol-depletion treatment with HP-β-cyclodextrin is a potential therapeutic strategy for NPC1 disease (Rosenbaum and Maxfield, 2011). We assessed whether this could also rescue the autophagy defects. Despite HP-β-cyclodextrin causing a dose-dependent reduction in cholesterol accumulation (Filipin staining) in $Npc1^{-/-}$ MEFs, it impaired autophagy, leading to dose- and time-dependent elevation in autophagosome/LC3-II and p62 levels (Figures 4D–4F and S4D–S4G). Similar results were obtained with 1% and 4% HP-β-cyclodextrin in rat primary cortical neurons (Figures 4G and S4H). Impairment of autophagy by HP-β-cyclodextrin is caused by inhibition of autophagosome maturation, causing a block in autophagic flux, as analyzed with the mRFP-GFP-LC3 reporter and bafA$_1$ assay (Figures 4H, 4I, and S4I). Low doses of HP-β-cyclodextrin, sufficient to deplete cholesterol, had a lesser impact on autophagy (Figures 4D–4F and S4E–S4G). HP-β-cyclodextrin-mediated accumulation of p62 was autophagy dependent because it had no effects in autophagy-deficient $Atg5^{-/-}$ MEFs (Figure 4J). However, endocytosis-mediated EGFR degradation remained unaffected, indicating that endosomal maturation and lysosomal proteolysis are not perturbed (Figure S4J). Thus, apart from NPC1 mutations causing cholesterol accumulation, sub-stantial depletion of cholesterol also impairs autophagy possibly due to changes in membrane lipid composition retarding the vesicle fusion events (Koga et al., 2010; Zhang et al., 2009). Thus, we infer a role for the NPC1 protein in mediating autophagic traffic independently of its effect on cholesterol handling.

Stimulation of Autophagy in NPC1 Mutant Cells Facilitates Autophagosome Maturation and Autophagic Cargo Clearance Independent of Amphisome Formation

Upregulation of autophagy is beneficial in several neurodegenerative diseases (Ravikumar et al., 2004; Rubinsztein et al., 2012; Sarkar, 2013; Sarkar et al., 2007). Using mTOR-dependent (starvation, rapamycin) and mTOR-independent (lithium) autophagy enhancers (Ravikumar et al., 2004; Sarkar et al., 2005; Blommaart et al., 1995), we assessed whether this approach will be rational in an NPC1 disease context and if autophagic flux can be restored in NPC1 mutant cells by measuring p62 clearance. Stimulating autophagy significantly reduced p62 and LC3-II/autophagosome levels in NPC1 mutant cells as a result of an increased autophagic flux (Figures 5A, 5B, and S5A–S5C). Restoration of functional autophagy under starvation in $Npc1^{-/-}$ MEFs is due to increased autophagosome maturation, as assessed with mRFP-GFP-LC3 reporter (Figure 5C). However, this process was independent of amphisome formation as indicated by reduced colocalization of LC3$^+$ and Rab7$^+$ vesicles, in contrast to starved $Npc1^{+/+}$ MEFs (Figures 2A, S2A, S2B, and S5D). Likewise, starvation or rapamycin reduced p62 levels in $Npc1^{-/-}$ MEFs with siRNA knockdown of VAMP8 (Figure S5E), which mediates amphisome formation (Itakura et al., 2012). Instead, autophagosomes possibly fused directly with the lysosomes during starvation-induced autophagy in $Npc1^{-/-}$ MEFs, as evident from increased colocalization between mRFP-LC3$^+$ and LAMP1-EGFP$^+$ vesicles (Figure 5D). Thus, stimulating autophagy could bypass the amphisome-forming vesicle fusion step to enable cargo clearance.

Starvation-induced autophagy also lowered p62 accumulation in $Npc1^{-/-}$ MEFs treated with a high dose (4%) of HP-β-cyclodextrin (Figures S5F and S5G) (depleted cholesterol by 85%–90% but further blocked autophagy; Figures 4D–4G and S4D–S4I), suggesting that combining a lower dose with autophagy enhancers may be rational to rescue both the cholesterol and autophagy defects. Indeed, $Npc1^{-/-}$ MEFs treated with 0.2% HP-β-cyclodextrin (depleted cholesterol by 40%–50% but not affecting autophagy; Figures 4D–4F and S4E–S4G) and

---

(D) Fluorescence staining and quantification of autophagosome (AP)-associated (mCherry$^+$-GFP$^+$-p62) and autolysosome (AL)-associated (mCherry$^+$-GFP$^-$-p62) p62 aggregates in $Npc1^{+/+}$ and $Npc1^{-/-}$ MEFs, expressing mCherry-GFP-p62 reporter for 24 hr, are shown. The scale bar represents 10 μm.

(E) Immunoblot analysis with anti-p62 and anti-actin antibodies in $Npc1^{+/+}$ and $Npc1^{-/-}$ MEFs, treated with or without 20 μg/ml cycloheximide (CHX) for 4, 8, 12, and 24 hr, is shown.

(F) Immunoblot analyses with anti-DJ-1, anti-Tom20, and anti-actin antibodies in $Npc1^{+/+}$ and $Npc1^{-/-}$ MEFs are shown. See also Figure S3I.

(G) Cell viability and apoptosis analysis with FITC-Annexin V and propidium iodide detection by FACS in $Npc1^{+/+}$ and $Npc1^{-/-}$ MEFs, treated with or without 10 μM CCCP for 18 hr, are shown.

(H) Fluorescence staining and quantification of FITC-dextran$^+$ and LysoTracker$^+$ structures, and their colocalization in $Npc1^{+/+}$ and $Npc1^{-/-}$ MEFs, incubated with Alexa Fluor 488 (FITC)-conjugated dextran for 3 hr followed by LysoTracker staining for 1 hr, are shown. The scale bar represents 10 μm.

(I) Immunoblot analyses with anti-cathepsin B, anti-cathepsin D, and anti-actin antibodies in $Npc1^{+/+}$ and $Npc1^{-/-}$ MEFs are shown.

(J) Immunofluorescence staining with anti-LAMP1 antibody in $Npc1^{+/+}$ and $Npc1^{-/-}$ MEFs is shown. The scale bar represents 10 μm.

(K) Cathepsin B activity in $Npc1^{+/+}$ and $Npc1^{-/-}$ MEFs, and in control and NPC1 patient fibroblasts, is shown. Cathepsin B activity is represented as μmole-free cathepsin B substrate (AMC) per μg of total protein per 30 min.

Graphical data denote mean ± SEM. ***p < 0.001, **p < 0.01, and *p < 0.05. ns, nonsignificant.
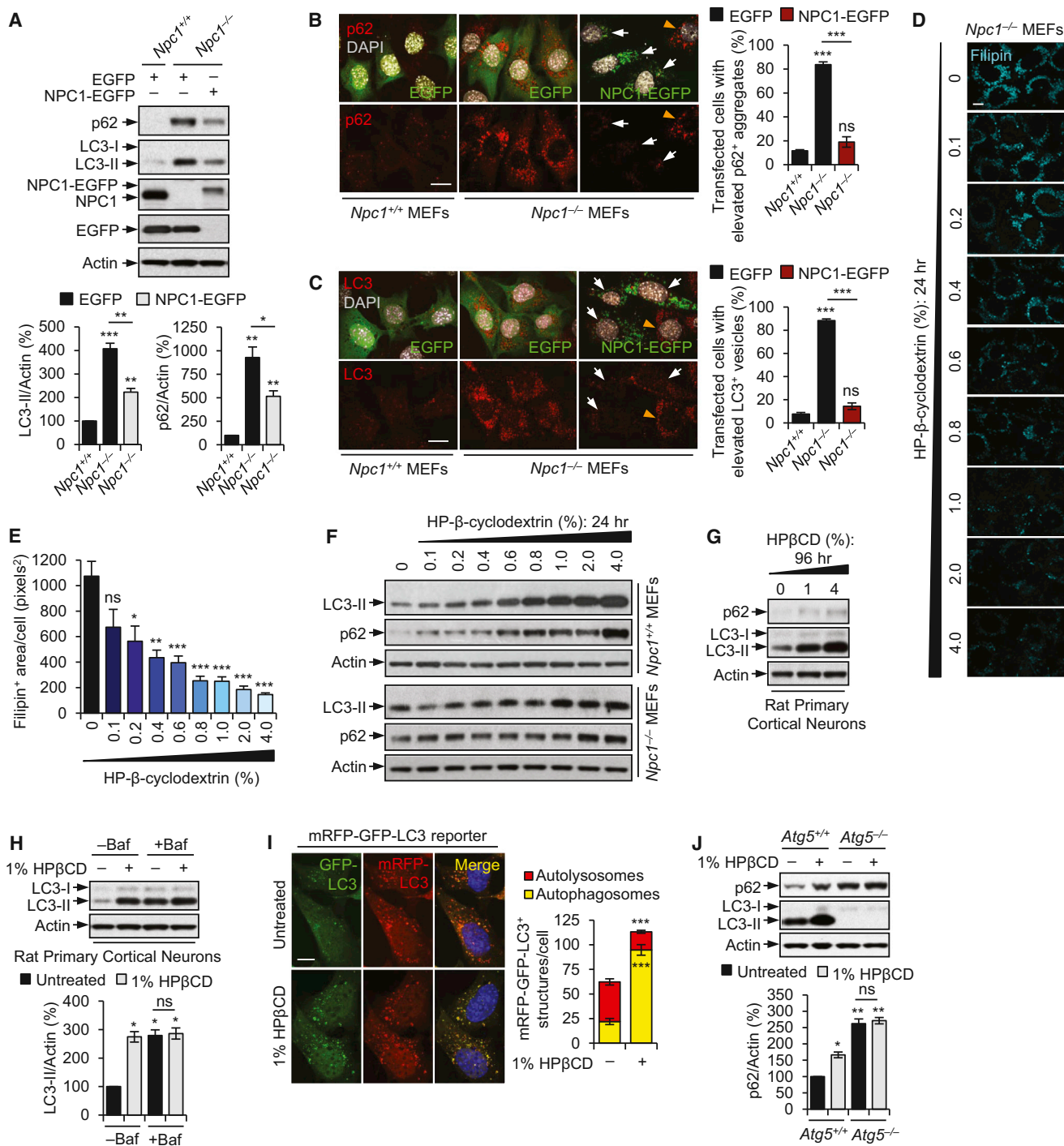
Figure 4. Rescue of Autophagy Defects in NPC1 Mutant Cells by Expressing Functional NPC1 Protein, whereas Cholesterol-Depletion Treatment Blocks Autophagic Flux

(A) Immunoblot analyses with anti-p62, anti-LC3, anti-NPC1, anti-EGFP, and anti-actin antibodies in $Npc1^{+/+}$ and $Npc1^{-/-}$ MEFs, expressing either *EGFP* or *NPC1-EGFP* for 48 hr, are shown.

(B and C) Immunofluorescence staining with anti-p62 (B) and anti-LC3 (C) antibodies, and quantification of cells exhibiting accumulated p62$^+$ aggregates (B) and LC3$^+$ vesicles (C) in $Npc1^{+/+}$ and $Npc1^{-/-}$ MEFs, expressing either *EGFP* or *NPC1-EGFP* for 48 hr, are presented. Arrows (white) show transfected cells, whereas arrowhead (orange) denotes a nontransfected cell. The scale bars represent 10 μm.

(D and E) Filipin staining (D) and quantification of Filipin intensity (E) in $Npc1^{-/-}$ MEFs, either left untreated or treated with 0.1%–4% HP-β-cyclodextrin for 24 hr, are shown. The scale bar represents 10 μm.

(legend continued on next page)

rapamycin or lithium significantly reduced p62 levels in the presence of HP-β-cyclodextrin (Figure 5E).

Inhibition of Autophagy Causes Cholesterol Accumulation, whereas Inducing Autophagy Increases Cell Viability in NPC1 Mutant Cells without Affecting Cholesterol Levels

Autophagy regulates lipid metabolism because abrogation of autophagy increases intracellular lipids in autophagy-deficient ($Atg5^{-/-}$) cells (Singh et al., 2009). We found that accumulation of cholesterol (Filipin staining) also occurred in $Atg5^{-/-}$ MEFs as well as in bafA$_1$-treated $Npc1^{+/+}$ MEFs, similar to the effects arising due to the loss of NPC1 protein in $Npc1^{-/-}$ MEFs (Figures 5F and 5G). Although 0.2% HP-β-cyclodextrin reduced cholesterol accumulation in $Npc1^{-/-}$ MEFs, stimulation of autophagy with rapamycin or lithium had no significant effect. Combining 0.2% HP-β-cyclodextrin with these autophagy inducers reduced cholesterol to what could be achieved with HP-β-cyclodextrin alone (Figures 5F and 5G). These data suggest that whereas inhibition of autophagy exhibits an NPC1-like cholesterol phenotype, activating autophagy in the context of NPC1 disease was unable to lower cholesterol levels.

We further examined the effects of HP-β-cyclodextrin and rapamycin on cellular viability in CCCP-treated $Npc1^{-/-}$ MEFs, which were more susceptible to apoptotic insults compared to $Npc1^{+/+}$ MEFs (Figures 3G and 5H). Although rapamycin, either alone or in combination with 0.2% HP-β-cyclodextrin, significantly rescued from cell death, 0.2% HP-β-cyclodextrin had no significant protective effects in $Npc1^{-/-}$ MEFs (Figure 5H). Thus, our data raise the possibility of activation of autophagy as a therapeutic strategy.

Defective Autophagic Flux In Vivo in Cerebellum and Liver of $Npc1^{-/-}$ Mice

Finally, we characterized defective autophagy in the organs primarily affected in NPC1 disease using cerebellum and liver from $Npc1^{-/-}$ mice (Loftus et al., 1997), where LC3-II and p62 levels were significantly elevated, thus confirming a block in autophagic flux in vivo (Figures 6A and 6B). Notably, similar to the clinical features of NPC1 disease, autophagy deficiency in the brain or liver of normal mice develops degeneration in Purkinje neurons or hepatocyte dysfunction, respectively (Hara et al., 2006; Komatsu et al., 2006, 2007). In addition, accumulation of p62 in autophagy-deficient mouse liver causes liver defects (Komatsu et al., 2010). Therefore, brain- and liver-specific interference with autophagy in mice associated with neurodegenera-

tion and liver injury suggests similar pathogenic consequences of impaired autophagy in NPC1 disease.

Induction of Autophagy Is Protective in a Neuronal Model of NPC1 Disease

To assess the efficacy of compounds in neurons, we used NPC1 knockdown cells to establish mouse neuronal cultures (Figure S6A). Because it is difficult to inhibit gene expression by shRNA in neurons, we initially infected mouse neural stem cells (mNSCs) (Nestin$^+$/Sox1$^+$; Figure S6B) with five independent lentiviral Npc1 shRNAs, with Npc1_2 shRNA being the most effective construct in reducing NPC1 protein levels (Figure 6C). Neural stem cells stably expressing Npc1_2 shRNA were then differentiated with retinoic acid into neurons (Robertson et al., 2008), which express the neuronal markers Tuj1 and MAP2 (Figures 6D and S6C). Consistent with our data, neurons expressing Npc1_2 shRNA had increased LC3$^+$ vesicles as well as LC3-II and p62 levels compared to control shRNA (Figures 6D and 6E), effects that were attributable to impaired autophagic flux as evident from the bafA$_1$ assay (Figure 6F). Likewise, NPC1 knockdown in neurons derived from human embryonic stem cells expressing NPC1 shRNA also displayed an increase in LC3-II levels (Ordonez et al., 2012).

Treatment of Npc1 knockdown mouse neurons (Npc1_2 shRNA) with rapamycin, either alone or in combination with 0.2% HP-β-cyclodextrin, significantly reduced p62 levels (Figure 6G). However, 0.2% HP-β-cyclodextrin had no effects on p62 clearance (Figure 6G), suggesting that its low dose does not perturb autophagic flux in neuronal culture. We further show that Npc1 knockdown neurons (Npc1_2 shRNA) were associated with increased cell death (Figures 6H and 6I). Notably, this deleterious effect was significantly rescued by rapamycin or 0.2% HP-β-cyclodextrin, whereas the combination treatment, although exhibiting the greatest protection, was not significantly better than rapamycin alone (Figure 6I). Thus, our data suggest that stimulation of autophagy may be beneficial for NPC1 disease and raise the possibility for a combination treatment approach with agents inducing autophagy and depleting cholesterol.

DISCUSSION

In summary, our data imply that the NPC1 protein functions at the crossroads of autophagy and endocytosis to regulate amphisome formation, and its loss of function predominantly impairs autophagy-specific traffic (Figures 7 and S7). This is attributable to a defective SNARE complex machinery, and it is likely that the

(F) Immunoblot analysis with anti-LC3, anti-p62, and anti-actin antibodies in $Npc1^{+/+}$ and $Npc1^{-/-}$ MEFs, treated with or without 0.1%–4% HP-β-cyclodextrin for 24 hr, is presented. Low exposures of immunoblots were shown to visualize changes in LC3-II and p62 levels. See also Figure S4E.

(G) Immunoblot analysis with anti-LC3, anti-p62, and anti-actin antibodies in rat primary cortical neurons, treated with or without 1% and 4% HP-β-cyclodextrin (HPβCD) for 96 hr, is shown. See also Figure S4H.

(H) Immunoblot analysis with anti-LC3 and anti-actin antibodies in rat primary cortical neurons, treated with or without 1% HP-β-cyclodextrin for 96 hr, in the presence or absence of 400 nM bafA$_1$ for the last 4 hr, is shown.

(I) Fluorescence staining and quantification of autophagosomes (mRFP$^+$-GFP$^+$-LC3) and autolysosomes (mRFP$^+$-GFP$^-$-LC3) in MEFs, expressing $mRFP$-$EGFP$-$LC3$ reporter for 24 hr and treated with or without 1% HP-β-cyclodextrin for 24 hr, are shown. The scale bar represents 10 μm.

(J) Immunoblot analysis with anti-LC3, anti-p62, and anti-actin antibodies in $Atg5^{+/+}$ and $Atg5^{-/-}$ MEFs, treated with or without 1% HP-β-cyclodextrin for 24 hr, is shown.

Graphical data denote mean ± SEM. ***$p < 0.001$, **$p < 0.01$, and *$p < 0.05$. ns, nonsignificant.
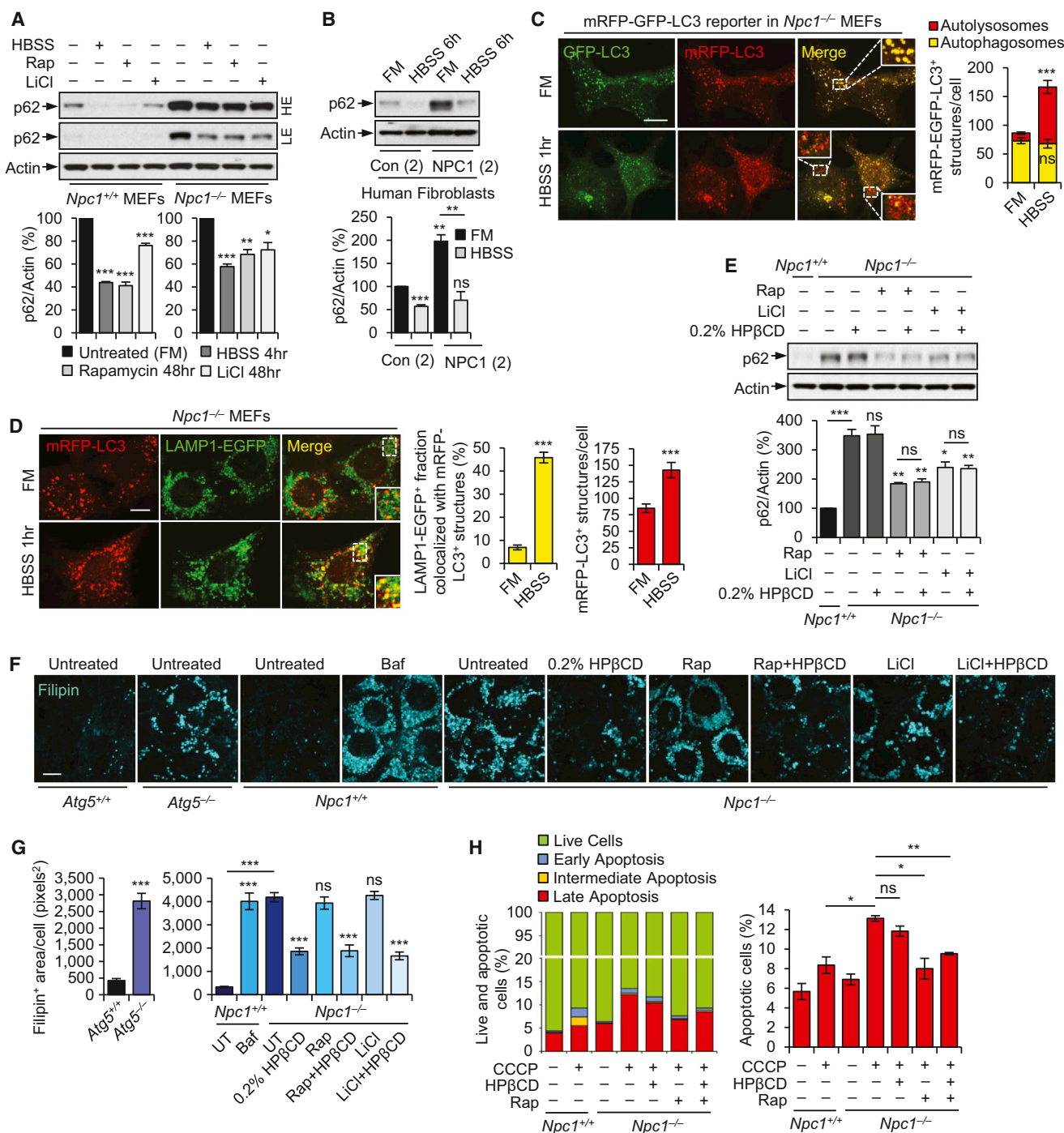
Figure 5. Simulating Autophagy Rescues Autophagy Defects in NPC1 Mutant Cells by Facilitating Autophagosome Maturation Independent of Amphisome Formation, whereas Abrogation of Autophagy Leads to Accumulation of Intracellular Cholesterol

(A) Immunoblot analysis with anti-p62 and anti-actin antibodies in $Npc1^{+/+}$ and $Npc1^{-/-}$ MEFs, cultured in FM with or without 400 nM rapamycin (Rap) or 10 mM lithium (LiCl) for 48 hr, or under starvation condition (HBSS; last 4 h), is presented. High exposure and low exposure of the same immunoblot are shown.

(B) Immunoblot analysis with anti-p62 and anti-actin antibodies in control and NPC1 patient fibroblasts, cultured either in basal (FM) or starvation (HBSS; 6 hr) condition, is shown.

(C) Fluorescence staining and quantification of autophagosomes (mRFP[+]-GFP[+]-LC3) and autolysosomes (mRFP[+]-GFP[−]-LC3) in $Npc1^{-/-}$ MEFs, expressing *mRFP-EGFP-LC3* reporter for 24 hr and cultured under basal (FM) or starvation (HBSS; last 1 hr) conditions, are shown. Cells were subjected to starvation for 1 hr to visualize LC3^{+} vesicles, instead of 4 hr where there was a substantial clearance of these vesicles (Figures S5B and S5C). The scale bar represents 10 μm.

(legend continued on next page)

LE/L-resident NPC1 protein plays a role in mediating membrane-tethering events between autophagosomes and late endosomes. Furthermore, abrogation of autophagy also causes cholesterol accumulation that mimics the mutant NPC1-like phenotype. Therefore, the underlying defect in autophagy in NPC1 disease may be deleterious and can act as a positive mediator for accumulating cholesterol. Additionally, brain- and liver-specific abrogation of basal autophagy in mice is associated with degeneration in the affected organs, which may imply similar pathogenic effects of defective autophagy in patients with NPC1 mutations.

Although autophagy upregulation is a potential treatment strategy for neurodegenerative disorders (Rubinsztein et al., 2012; Sarkar, 2013), the utility of such an approach for lipid-/lysosomal-storage diseases is not clear (Lieberman et al., 2012). Our study reveals that stimulating autophagy in the context of NPC1 disease can restore the clearance of autophagic cargo by mediating autophagosome-lysosome fusion independent of amphisome formation (Figure 7), which also suggests that the lysosomal proteolysis is functional. Our findings argue against inhibition of autophagy as a therapeutic strategy as reported recently by Ordonez et al. (2012) because such treatment may perturb its vital housekeeping functions (Hara et al., 2006; Komatsu et al., 2006, 2007, 2010; Ravikumar et al., 2010; Singh et al., 2009).

Our data suggest that stimulating autophagy does not rescue the cholesterol phenotype in NPC1 mutant cells, possibly because cholesterol is trapped in late endosomal compartments, whereas facilitating direct autophagosome-lysosome fusion restores functional autophagy. On the other hand, HP-β-cyclodextrin serves as cholesterol-depletion agent for NPC1 disease (Rosenbaum and Maxfield, 2011). Because HP-β-cyclodextrin also blocks autophagic flux, and with high doses being neurotoxic (Peake and Vance, 2012), our data emphasize the need for careful dosing of this drug. Thus, a low dose of HP-β-cyclodextrin that partially depletes cholesterol without perturbing autophagy, coupled with an autophagy inducer that restores autophagic flux by overcoming its block, may provide a rational combination treatment strategy for NPC1 disease. We have validated some of these clinically relevant observations in human hepatocytes derived from NPC1 patient-specific-induced pluripotent stem cells, where impaired autophagy is rescued by small molecules enhancing autophagy (D.M., S.S., H.W., and R.J., unpublished data). Our study points to upregulating autophagy as a possible therapeutic strategy for the treatment of lipid-/lysosomal-storage disorders.

EXPERIMENTAL PROCEDURES

Details of Experimental Procedures can be found in Supplemental Experimental Procedures.

Culture of Mammalian Cells, Neural Stem Cells, and Primary Cortical Neurons
Culture of $Npc1^{+/+}$ and $Npc1^{-/-}$ MEFs (Loftus et al., 1997) (gift from Peter Lobel), $Atg5^{+/+}$ and $Atg5^{-/-}$ MEFs (Kuma et al., 2004) (gift from Noboru Mizushima), Human embryonic kidney 293T cells, rat primary cortical neurons, mNSCs, and neuronal culture derived from mNSCs are described in the Supplemental Experimental Procedures.

Immunoblot Analysis
Cell lysates were subjected to western blot, as previously described (Sarkar et al., 2009). See the Supplemental Experimental Procedures for details and a list of primary antibodies.

Immunofluorescence and Image Analysis
Cells were fixed with 4% paraformaldehyde, permeabilized, and incubated with primary antibodies, as detailed in the Supplemental Experimental Procedures. Image analysis was performed using ImageJ software (NIH), as described in the Supplemental Experimental Procedures.

Filipin and BODIPY Staining for Detecting Cholesterol and Lipid Accumulation
Cholesterol accumulation in cells was visualized with Filipin staining (Filipin complex from *Streptomyces filipinensis*; F9765, Sigma-Aldrich). After paraformaldehyde fixation, cells were incubated with 1.5 mg/ml glycine for 10 min and incubated in 50 μg/ml Filipin for 2–3 hr at room temperature. Accumulation of neutral lipids in cells was visualized with BODIPY 493/503 staining (Singh et al., 2009) (4,4-Difluoro-1,3,5,7,8-Pentamethyl-4-Bora-3a,4a-Diaza-s-Indacene; D-3922, Life Technologies). Cells were incubated with 1 μM BODIPY 493/503 in FM for 1 hr prior to paraformaldehyde fixation.

MS Analysis
Whole-cell lysates of $Npc1^{+/+}$ and $Npc1^{-/-}$ MEFs from triplicate experiments were subjected to MS analysis. Sample preparation, chromatographic separations, MS, and data analysis are detailed in the Supplemental Experimental Procedures.

Autophagy Analyses
Analysis of Autophagosome Synthesis with bafA₁
Autophagosome synthesis was analyzed by measuring LC3-II levels (immunoblotting with anti-LC3 antibody) in the presence of 400 nM bafA₁, as previously described (Sarkar et al., 2009). See the Supplemental Experimental Procedures for details.
Analysis of Autophagic Flux with mRFP-GFP-LC3 Reporter
Autophagosomes (mRFP⁺-GFP⁺-LC3) and autolysosomes (mRFP⁺-GFP⁻-LC3) were quantified by ImageJ software using parameters as previously described by Kimura et al. (2007). See the Supplemental Experimental Procedures for details.

(D) Fluorescence staining and quantification of mRFP-LC3⁺ vesicles and their colocalization with LAMP1-EGFP⁺ structures in $NPC1^{-/-}$ MEFs expressing *mRFP-LC3* and *LAMP1-EGFP* for 24 hr, cultured either in basal (FM) or starvation (HBSS; last 1 hr) condition, are shown. Cells were subjected to starvation-induced autophagy for 1 hr as explained above. The scale bar represents 10 μm.
(E) Immunoblot analysis with anti-p62 and anti-actin antibodies in $Npc1^{+/+}$ and $Npc1^{-/-}$ MEFs, where $Npc1^{-/-}$ MEFs were treated with or without 400 nM rapamycin or 10 mM lithium for 48 hr, in the presence or absence of 0.2% HP-β-cyclodextrin for the last 24 hr, is shown.
(F and G) Filipin staining (F) and quantification of Filipin intensity (G) in $Atg5^{+/+}$ and $Atg5^{-/-}$ MEFs, $Npc1^{+/+}$ MEFs treated with or without 400 nM bafA₁ (24 hr), and in $Npc1^{-/-}$ MEFs, either left untreated (UT) or treated with 200 nM rapamycin (48 hr), 10 mM lithium (48 hr), 0.2% HP-β-cyclodextrin (24 hr), or a combination of compounds as indicated, are shown. The scale bar represents 10 μm.
(H) Cell viability and apoptosis analysis with FITC-Annexin V and propidium iodide detection by FACS in $Npc1^{+/+}$ and $Npc1^{-/-}$ MEFs, treated with or without 200 nM rapamycin, 0.2% HP-β-cyclodextrin, or both for 48 hr, in the presence or absence of 10 μM CCCP for the last 18 hr, are shown.
Graphical data denote mean ± SEM. ***$p < 0.001$, **$p < 0.01$, and *$p < 0.05$. ns, nonsignificant.
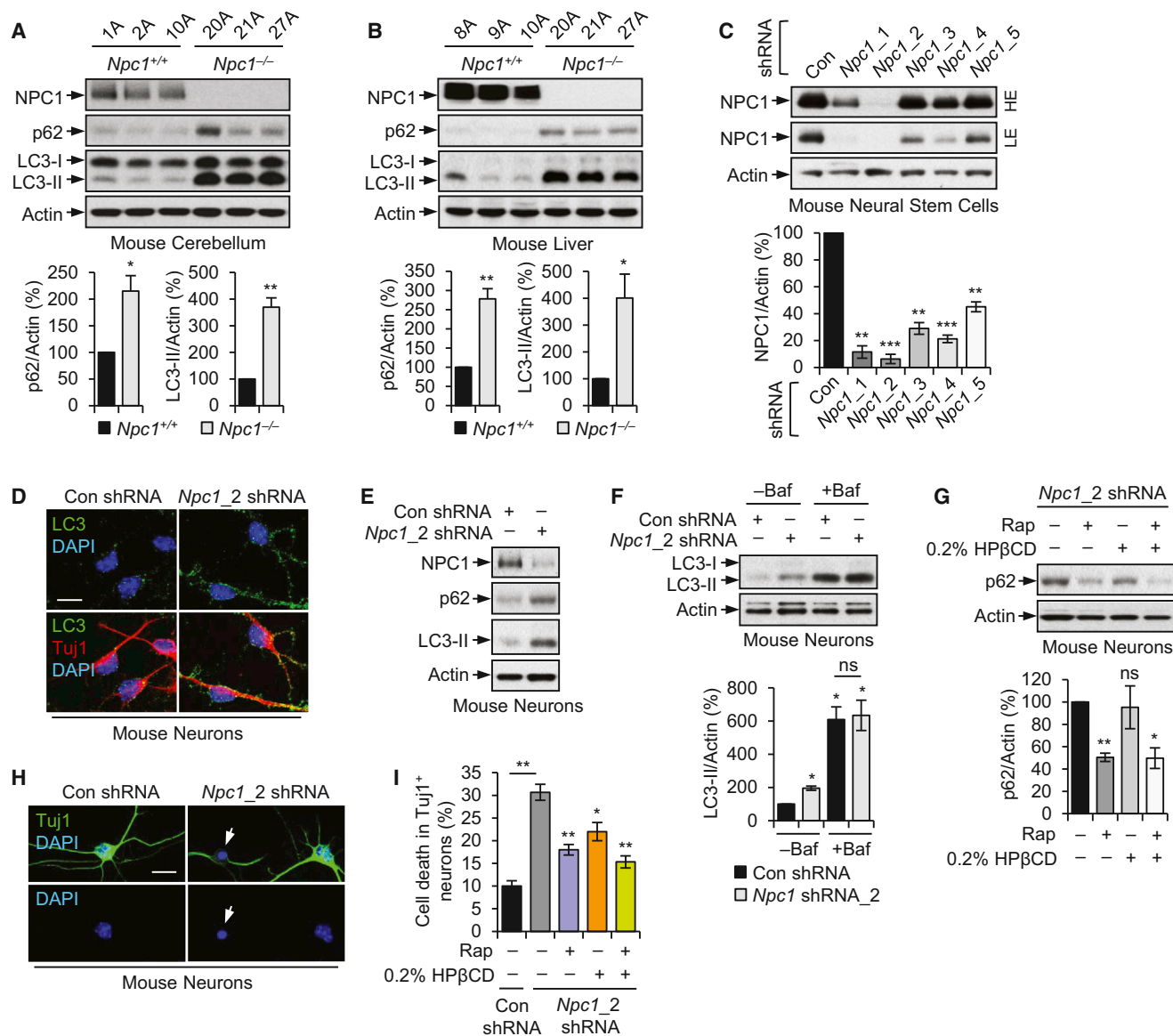
Figure 6. Impaired Autophagic Flux In Vivo in Organs from $Npc1^{-/-}$ Mice and Rescue of Cell Death in Neurons with NPC1 Knockdown

(A and B) Immunoblot analyses with anti-NPC1, anti-p62, anti-LC3, and anti-actin antibodies in cerebellum (A) and liver (B) tissues from $Npc1^{+/+}$ and $Npc1^{-/-}$ mice are shown.

(C) Immunoblot analyses with anti-NPC1, and anti-actin antibodies in primary mNSCs transduced with five different lentiviral $Npc1$ shRNAs or control shRNA are presented. High and low exposures of the same immunoblot are shown. Densitometric analysis was done on low exposures of immunoblots. Schematic representation of generating NPC1 knockdown neuronal cells is shown in Figure S6A.

(D) Immunofluorescence staining with anti-LC3 and anti-Tuj1 antibodies in neurons differentiated from mNSCs expressing control or $Npc1\_2$ shRNA is shown. The scale bar represents 10 μm.

(E) Immunoblot analyses with anti-NPC1, anti-p62, anti-LC3, and anti-actin in neurons differentiated from mNSCs expressing control or $Npc1\_2$ shRNA are shown.

(F) Immunoblot analysis with anti-LC3 and anti-actin antibodies in neurons differentiated from mNSCs expressing control or $Npc1\_2$ shRNA, treated with or without 400 nM bafA$_1$ for 4 hr, is shown.

(G) Immunoblot analysis with anti-p62 and anti-actin antibodies in neurons differentiated from mNSCs expressing $Npc1\_2$ shRNA, treated with or without 200 nM rapamycin, 0.2% HP-β-cyclodextrin, or both for 72 hr, is shown.

(H) Immunofluorescence staining with anti-Tuj1 antibody in neurons differentiated from mNSCs expressing control or $Npc1\_2$ shRNA is presented. Nuclei were stained with DAPI, and arrows show an apoptotic nucleus. The scale bar represents 10 μm.

(I) Analysis of cell death in Tuj1$^+$ neurons differentiated from mNSCs expressing control or $Npc1\_2$ shRNA, where neurons with NPC1 knockdown were treated with or without 200 nM rapamycin, 0.2% HP-β-cyclodextrin, or both for 72 hr, is presented.

Graphical data denote mean ± SEM. ***$p < 0.001$, **$p < 0.01$, and *$p < 0.05$. ns, nonsignificant.
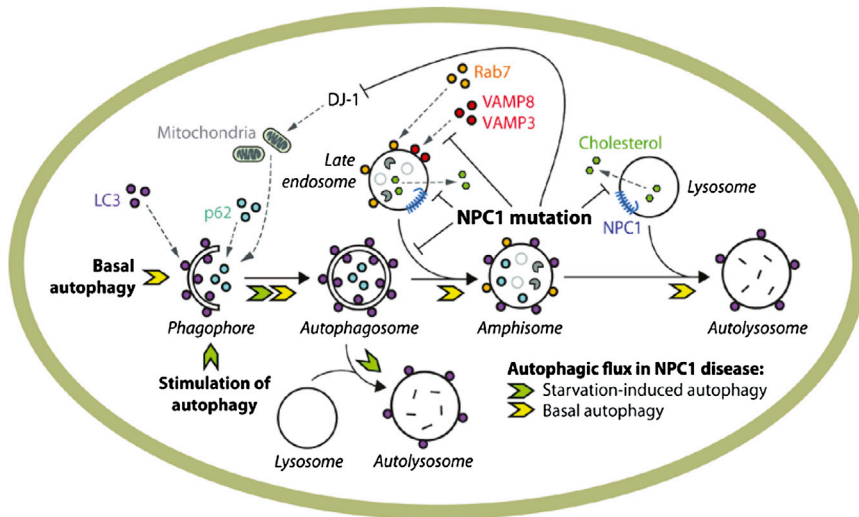
Figure 7. Schematic Representation of Defective Autophagy and the Effects of Its Stimulation in NPC1 Disease

Mutations in the NPC1 protein inhibit cholesterol efflux and accumulate cholesterol in the LE/L compartments. Additionally, mutations in the NPC1 protein impair autophagosome maturation, leading to a block in autophagy associated with accumulation of autophagosomes (LC3$^+$ vesicles) and autophagy substrates (p62 and mitochondria). This is attributed to defective amphisome formation where the autophagosomes fail to fuse with late endosomes (Rab7$^+$ vesicles) due to the inability of NPC1-deficient late endosomes to recruit components of SNARE machinery, such as VAMP8 and VAMP3, which regulate this fusion event. NPC1 mutations also deplete DJ-1, leading to mitochondrial fragmentation and accumulation of damaged mitochondria due to impaired mitophagy. Upregulation of autophagy (such as by starvation and small molecules) bypasses the autophagy block in NPC1 mutant cells and rescues the autophagy defects by facilitating autophagosome maturation through their fusion with the lysosomes independent of amphisome formation, thereby mediating the clearance of autophagic cargo. Overview of perturbations in the autophagy pathway in NPC1 disease is listed in Figure S7.

Analysis of Autophagic Cargo Flux with mCherry-GFP-p62 Reporter

p62 aggregates associated with autophagosomes (mRFP$^+$-GFP$^+$-p62) and autolysosomes (mRFP$^+$-GFP$^-$-p62) were quantified by ImageJ software using parameters as previously described by Pankiv et al. (2007). See the Supplemental Experimental Procedures for details.

Statistical Analyses

Densitometry analyses on the immunoblots from multiple experiments were performed by ImageJ software, as previously described (Sarkar et al., 2007, 2009). The control condition was set to 100%, and the data represented mean ± SEM. The p values for various analyses were determined by Student's t test (unpaired) using Prism 6 software (GraphPad): ***$p < 0.001$, **$p < 0.01$, and * $p < 0.05$ ("ns" indicates nonsignificant).

SUPPLEMENTAL INFORMATION

Supplemental Information includes Supplemental Experimental Procedures and seven figures and can be found with this article online at http://dx.doi.org/10.1016/j.celrep.2013.10.042.

REFERENCES

Berg, T.O., Fengsrud, M., Strømhaug, P.E., Berg, T., and Seglen, P.O. (1998). Isolation and characterization of rat liver amphisomes. Evidence for fusion of autophagosomes with both early and late endosomes. J. Biol. Chem. *273*, 21883–21892.

Blommaart, E.F., Luiken, J.J., Blommaart, P.J., van Woerkom, G.M., and Meijer, A.J. (1995). Phosphorylation of ribosomal protein S6 is inhibitory for autophagy in isolated rat hepatocytes. J. Biol. Chem. *270*, 2320–2326.

Carstea, E.D., Morris, J.A., Coleman, K.G., Loftus, S.K., Zhang, D., Cummings, C., Gu, J., Rosenfeld, M.A., Pavan, W.J., Krizman, D.B., et al. (1997). Niemann-Pick C1 disease gene: homology to mediators of cholesterol homeostasis. Science *277*, 228–231.

Elrick, M.J., Yu, T., Chung, C., and Lieberman, A.P. (2012). Impaired proteolysis underlies autophagic dysfunction in Niemann-Pick type C disease. Hum. Mol. Genet. *21*, 4876–4887.

Fader, C.M., Sánchez, D.G., Mestre, M.B., and Colombo, M.I. (2009). TI-VAMP/VAMP7 and VAMP3/cellubrevin: two v-SNARE proteins involved in specific steps of the autophagy/multivesicular body pathways. Biochim. Biophys. Acta *1793*, 1901–1916.

Hara, T., Nakamura, K., Matsui, M., Yamamoto, A., Nakahara, Y., Suzuki-Migishima, R., Yokoyama, M., Mishima, K., Saito, I., Okano, H., and Mizushima, N. (2006). Suppression of basal autophagy in neural cells causes neurodegenerative disease in mice. Nature *441*, 885–889.

Higgins, M.E., Davies, J.P., Chen, F.W., and Ioannou, Y.A. (1999). Niemann-Pick C1 is a late endosome-resident protein that transiently associates with lysosomes and the trans-Golgi network. Mol. Genet. Metab. *68*, 1–13.

Ikonen, E. (2008). Cellular cholesterol trafficking and compartmentalization. Nat. Rev. Mol. Cell Biol. *9*, 125–138.

Ishibashi, S., Yamazaki, T., and Okamoto, K. (2009). Association of autophagy with cholesterol-accumulated compartments in Niemann-Pick disease type C cells. J. Clin. Neurosci. *16*, 954–959.

Itakura, E., Kishi-Itakura, C., and Mizushima, N. (2012). The hairpin-type tail-anchored SNARE syntaxin 17 targets to autophagosomes for fusion with endosomes/lysosomes. Cell *151*, 1256–1269.

Jäger, S., Bucci, C., Tanida, I., Ueno, T., Kominami, E., Saftig, P., and Eskelinen, E.-L. (2004). Role for Rab7 in maturation of late autophagic vacuoles. J. Cell Sci. *117*, 4837–4848.

Kabeya, Y., Mizushima, N., Ueno, T., Yamamoto, A., Kirisako, T., Noda, T., Kominami, E., Ohsumi, Y., and Yoshimori, T. (2000). LC3, a mammalian homologue of yeast Apg8p, is localized in autophagosome membranes after processing. EMBO J. *19*, 5720–5728.

Karten, B., Peake, K.B., and Vance, J.E. (2009). Mechanisms and consequences of impaired lipid trafficking in Niemann-Pick type C1-deficient mammalian cells. Biochim. Biophys. Acta 1791, 659–670.

Kimura, S., Noda, T., and Yoshimori, T. (2007). Dissection of the autophagosome maturation process by a novel reporter protein, tandem fluorescent-tagged LC3. Autophagy 3, 452–460.

Klionsky, D.J., Abdalla, F.C., Abeliovich, H., Abraham, R.T., Acevedo-Arozena, A., Adeli, K., Agholme, L., Agnello, M., Agostinis, P., Aguirre-Ghiso, J.A., et al. (2012). Guidelines for the use and interpretation of assays for monitoring autophagy. Autophagy 8, 445–544.

Kobayashi, T., Beuchat, M.H., Lindsay, M., Frias, S., Palmiter, R.D., Sakuraba, H., Parton, R.G., and Gruenberg, J. (1999). Late endosomal membranes rich in lysobisphosphatidic acid regulate cholesterol transport. Nat. Cell Biol. 1, 113–118.

Koga, H., Kaushik, S., and Cuervo, A.M. (2010). Altered lipid content inhibits autophagic vesicular fusion. FASEB J. 24, 3052–3065.

Komatsu, M., Waguri, S., Chiba, T., Murata, S., Iwata, J.I., Tanida, I., Ueno, T., Koike, M., Uchiyama, Y., Kominami, E., and Tanaka, K. (2006). Loss of autophagy in the central nervous system causes neurodegeneration in mice. Nature 441, 880–884.

Komatsu, M., Waguri, S., Koike, M., Sou, Y.S., Ueno, T., Hara, T., Mizushima, N., Iwata, J., Ezaki, J., Murata, S., et al. (2007). Homeostatic levels of p62 control cytoplasmic inclusion body formation in autophagy-deficient mice. Cell 131, 1149–1163.

Komatsu, M., Kurokawa, H., Waguri, S., Taguchi, K., Kobayashi, A., Ichimura, Y., Sou, Y.S., Ueno, I., Sakamoto, A., Tong, K.I., et al. (2010). The selective autophagy substrate p62 activates the stress responsive transcription factor Nrf2 through inactivation of Keap1. Nat. Cell Biol. 12, 213–223.

Korolchuk, V.I., Mansilla, A., Menzies, F.M., and Rubinsztein, D.C. (2009). Autophagy inhibition compromises degradation of ubiquitin-proteasome pathway substrates. Mol. Cell 33, 517–527.

Kuma, A., Hatano, M., Matsui, M., Yamamoto, A., Nakaya, H., Yoshimori, T., Ohsumi, Y., Tokuhisa, T., and Mizushima, N. (2004). The role of autophagy during the early neonatal starvation period. Nature 432, 1032–1036.

Kwon, H.J., Abi-Mosleh, L., Wang, M.L., Deisenhofer, J., Goldstein, J.L., Brown, M.S., and Infante, R.E. (2009). Structure of N-terminal domain of NPC1 reveals distinct subdomains for binding and transfer of cholesterol. Cell 137, 1213–1224.

Lieberman, A.P., Puertollano, R., Raben, N., Slaugenhaupt, S., Walkley, S.U., and Ballabio, A. (2012). Autophagy in lysosomal storage disorders. Autophagy 8, 719–730.

Loftus, S.K., Morris, J.A., Carstea, E.D., Gu, J.Z., Cummings, C., Brown, A., Ellison, J., Ohno, K., Rosenfeld, M.A., Tagle, D.A., et al. (1997). Murine model of Niemann-Pick C disease: mutation in a cholesterol homeostasis gene. Science 277, 232–235.

Meijer, A.J., and Codogno, P. (2006). Signalling and autophagy regulation in health, aging and disease. Mol. Aspects Med. 27, 411–425.

Millard, E.E., Srivastava, K., Traub, L.M., Schaffer, J.E., and Ory, D.S. (2000). Niemann-pick type C1 (NPC1) overexpression alters cellular cholesterol homeostasis. J. Biol. Chem. 275, 38445–38451.

Mizushima, N., Levine, B., Cuervo, A.M., and Klionsky, D.J. (2008). Autophagy fights disease through cellular self-digestion. Nature 451, 1069–1075.

Ordonez, M.P., Roberts, E.A., Kidwell, C.U., Yuan, S.H., Plaisted, W.C., and Goldstein, L.S. (2012). Disruption and therapeutic rescue of autophagy in a human neuronal model of Niemann Pick type C1. Hum. Mol. Genet. 21, 2651–2662.

Pacheco, C.D., Kunkel, R., and Lieberman, A.P. (2007). Autophagy in Niemann-Pick C disease is dependent upon Beclin-1 and responsive to lipid trafficking defects. Hum. Mol. Genet. 16, 1495–1503.

Pankiv, S., Clausen, T.H., Lamark, T., Brech, A., Bruun, J.A., Outzen, H., Øvervatn, A., Bjørkøy, G., and Johansen, T. (2007). p62/SQSTM1 binds directly to Atg8/LC3 to facilitate degradation of ubiquitinated protein aggregates by autophagy. J. Biol. Chem. 282, 24131–24145.

Peake, K.B., and Vance, J.E. (2012). Normalization of cholesterol homeostasis by 2-hydroxypropyl-β-cyclodextrin in neurons and glia from Niemann-Pick C1 (NPC1)-deficient mice. J. Biol. Chem. 287, 9290–9298.

Ravikumar, B., Vacher, C., Berger, Z., Davies, J.E., Luo, S., Oroz, L.G., Scaravilli, F., Easton, D.F., Duden, R., O'Kane, C.J., and Rubinsztein, D.C. (2004). Inhibition of mTOR induces autophagy and reduces toxicity of polyglutamine expansions in fly and mouse models of Huntington disease. Nat. Genet. 36, 585–595.

Ravikumar, B., Berger, Z., Vacher, C., O'Kane, C.J., and Rubinsztein, D.C. (2006). Rapamycin pre-treatment protects against apoptosis. Hum. Mol. Genet. 15, 1209–1216.

Ravikumar, B., Sarkar, S., Davies, J.E., Futter, M., Garcia-Arencibia, M., Green-Thompson, Z.W., Jimenez-Sanchez, M., Korolchuk, V.I., Lichtenberg, M., Luo, S., et al. (2010). Regulation of mammalian autophagy in physiology and pathophysiology. Physiol. Rev. 90, 1383–1435.

Robertson, M.J., Gip, P., and Schaffer, D.V. (2008). Neural stem cell engineering: directed differentiation of adult and embryonic stem cells into neurons. Front. Biosci. 13, 21–50.

Rosenbaum, A.I., and Maxfield, F.R. (2011). Niemann-Pick type C disease: molecular mechanisms and potential therapeutic approaches. J. Neurochem. 116, 789–795.

Rubinsztein, D.C., Codogno, P., and Levine, B. (2012). Autophagy modulation as a potential therapeutic target for diverse diseases. Nat. Rev. Drug Discov. 11, 709–730.

Sarkar, S. (2013). Regulation of autophagy by mTOR-dependent and mTOR-independent pathways: autophagy dysfunction in neurodegenerative diseases and therapeutic application of autophagy enhancers. Biochem. Soc. Trans. 41, 1103–1130.

Sarkar, S., Floto, R.A., Berger, Z., Imarisio, S., Cordenier, A., Pasco, M., Cook, L.J., and Rubinsztein, D.C. (2005). Lithium induces autophagy by inhibiting inositol monophosphatase. J. Cell Biol. 170, 1101–1111.

Sarkar, S., Perlstein, E.O., Imarisio, S., Pineau, S., Cordenier, A., Maglathlin, R.L., Webster, J.A., Lewis, T.A., O'Kane, C.J., Schreiber, S.L., and Rubinsztein, D.C. (2007). Small molecules enhance autophagy and reduce toxicity in Huntington's disease models. Nat. Chem. Biol. 3, 331–338.

Sarkar, S., Ravikumar, B., and Rubinsztein, D.C. (2009). Autophagic clearance of aggregate-prone proteins associated with neurodegeneration. Methods Enzymol. 453, 83–110.

Singh, R., Kaushik, S., Wang, Y., Xiang, Y., Novak, I., Komatsu, M., Tanaka, K., Cuervo, A.M., and Czaja, M.J. (2009). Autophagy regulates lipid metabolism. Nature 458, 1131–1135.

Sleat, D.E., Wiseman, J.A., Sohar, I., El-Banna, M., Zheng, H., Moore, D.F., and Lobel, P. (2012). Proteomic analysis of mouse models of Niemann-Pick C disease reveals alterations in the steady-state levels of lysosomal proteins within the brain. Proteomics 12, 3499–3509.

Stenmark, H. (2009). Rab GTPases as coordinators of vesicle traffic. Nat. Rev. Mol. Cell Biol. 10, 513–525.

Thomas, K.J., McCoy, M.K., Blackinton, J., Beilina, A., van der Brug, M., Sandebring, A., Miller, D., Maric, D., Cedazo-Minguez, A., and Cookson, M.R. (2011). DJ-1 acts in parallel to the PINK1/parkin pathway to control mitochondrial function and autophagy. Hum. Mol. Genet. 20, 40–50.

Youle, R.J., and Narendra, D.P. (2011). Mechanisms of mitophagy. Nat. Rev. Mol. Cell Biol. 12, 9–14.

Zhang, J., Xue, R., Ong, W.Y., and Chen, P. (2009). Roles of cholesterol in vesicle fusion and motion. Biophys. J. 97, 1371–1380.